
STATE-DEPENDENT FORCES IN COLD QUANTUM GASES

Christopher Billington

Submitted in total fulfilment of the requirements
of the degree of Doctor of Philosophy

Supervisory committee:

Prof Kristian Helmerson

Dr Lincoln Turner

Dr Russell Anderson



School of Physics and Astronomy
Monash University

January, 2017

rev: 89 (d42828f15099)
author: Chris Billington
date: Tue Oct 17 17:39:06 2017 -0400
summary: Merge

This page intentionally left blank

Contents

Contents	i
2 Atomic physics: Experimental techniques and theory	1
2.1 Cooling, trapping, and manipulating atoms	1
2.1.1 Doppler cooling	2
2.1.2 Magneto-optical and magnetic trapping	2
2.1.3 Optical trapping	2
2.1.4 Polarisation gradient cooling	3
2.1.5 Evaporative cooling	3
2.1.6 Feshbach resonances	4
2.2 Mean field theory: The Gross–Pitaevskii equation and vortices	4
2.3 Optical transitions on the ^{87}Rb D line	6
2.3.1 Fine structure	6
2.3.2 Hyperfine structure	7
2.3.3 Zeeman sublevels	11
2.3.4 Putting it all together	12
References	15

rev: 89 (d42828f15099)
author: Chris Billington
date: Tue Oct 17 17:39:06 2017 -0400
summary: Merge

This page intentionally left blank

rev: 89 (d42828f15099)
author: Chris Billington
date: Tue Oct 17 17:39:06 2017 -0400
summary: Merge

Atomic physics: Experimental techniques and theory

- Descriptions of the relevant physics in atomic physics experiments: Doppler cooling and magneto-optical traps, Sisyphus cooling, dipole forces, Feshbach resonances, scattering theory, Bose–Einstein statistics. Show how the Hamiltonian of a ‘two level’ (3/2 levels, all things considered for ^{87}Rb D line) atom with fine structure, hyperfine structure and Zeeman splitting arises from consideration of the different angular momenta. Use this to derive the differential equations for the state populations of an atom in a driving laser field. Gross Pitaevskii equation for single species, dual species and spinor condensate.
- Doppler cooling
- Magneto-optical trapping
- Optical dipole trapping
- Two-body scattering and Feshbach resonances
- -> Include stuff from 3rd year report
- Spin, fine structure, and hyperfine structure
- Equations of motion for two level atom with hyperfine structure
- The Monte-Carlo wavefunction method
- Mean field theory for Bose–Einstein condensates
- -> Superfluid velocity
- -> Vortices

2.1 Cooling, trapping, and manipulating atoms

BECs provide such a tantalising opportunity for studying quantum phenomena not only because of their interesting properties, but also because of the level of control they afford. Many of the same techniques which allow experimentalists such control over their creation are also employed in the creation thereof, and many were discovered along the way to Bose–Einstein condensation.

rev: 89 (d42828f15099)
 author: Chris Billington
 date: Tue Oct 17 17:39:06 2017 -0400
 summary: Merge

The main experimental techniques used to create BEC—and which we are and will be employing in that pursuit—are Doppler cooling, magneto-optical and dipole trapping, polarisation gradient (Sisyphus) cooling, and evaporative cooling.

These were discovered, perhaps by no coincidence, in roughly the same order as they are called for in a BEC experiment.

2.1.1 Doppler cooling

Doppler cooling, demonstrated in 1978 [?] is a consequence of the simple observation that atoms see the wavelength of incident light Doppler shifted depending on their velocity. This can be used to selectively transfer momentum to only fast-moving atoms, by tuning an incident laser slightly redder than would be required for a resonant absorption. If six lasers in counterpropagating pairs orthogonal to each other surround a cloud of atoms, the atoms can be cooled close to the *Doppler limit* [?, p 58]

$$k_B T_D = \frac{\hbar \Gamma}{2} \quad (2.1)$$

where Γ is the linewidth of the atomic transition. For the cooling transition used for Doppler cooling ^{87}Rb ¹, this gives 146 μK , which is approximately a factor of a thousand too high for Bose-condensation. These atoms are also not trapped.

¹The D_2 line, $5S_{\frac{1}{2}} \rightarrow 5P_{\frac{3}{2}}$, approximately 780 nm.

2.1.2 Magneto-optical and magnetic trapping

Magneto-optical trapping, first demonstrated in 1987 [?] comes from the realisation that a magnetic field can be used to *spatially* vary the detuning from resonance that the atoms in the above mentioned arrangement of lasers see. This is possible due to the Zeeman effect [?], in which the wavelengths of atomic transitions are shifted in a magnetic field.

If a field profile can be found which causes the transition to come closer to resonance as the atoms move away from a central point, then it forms a trap—atoms that stray too far from the centre will absorb more strongly and be deflected back².

The field configuration used in an anti-Helmholtz one, with two coils opposite each other carrying opposing currents. The resulting magnetic field profile has a zero in the middle and increases in magnitude in all directions.

With the Doppler beams off, this magnetic field still provides a trapping potential, due to the magnetic dipole interaction:

$$V(\mathbf{r}) = -\boldsymbol{\mu} \cdot \mathbf{B}, \quad (2.2)$$

where $\boldsymbol{\mu}$ is the atomic magnetic moment, and \mathbf{B} the magnetic field. This only traps some atomic spin states, and has losses due to spin-flips [?] near the field zero.

2.1.3 Optical trapping

Optical dipole trapping on the other hand relies on the *dipole force*, in which off-resonant light shifts the energy of the eigenstates of the combined atom-light system, the so called *dressed states*. This energy shift, called the *light shift*, depends on the intensity of the light, and so results in a potential that spatially varies as the intensity of the light. In the limit of large detuning (compared to Rabi frequency), this shift is given by [?, p 8]:

$$\Delta E = \frac{\hbar \Omega^2}{4\delta} \quad (2.3)$$

where δ is the detuning from resonance and the Rabi frequency is:

$$\Omega = \frac{eE_0}{\hbar} \langle 1|x|2 \rangle, \quad (2.4)$$

²The polarisations of the beams are such that absorption from the inward facing beam occurs, rather than from the one that would accelerate the atom further outward!

where E_0 is the amplitude of the light's electric field and $\langle 1|x|2 \rangle$ is the dipole moment between the two states in a two-level system.

With the potential proportional to E_0^2 , and thus the light's intensity, the force the atom experiences is proportional to the light's intensity gradient. For this reason, the dipole force is also called the *gradient force*. The name *dipole force* comes from the fact that the force can be equivalently understood to arise from the polarisability of atoms in a light field, giving rise to a force identical to that which traps polarisable materials in optical tweezers [?].

2.1.4 Polarisation gradient cooling

Polarisation gradient cooling, also called Sisyphus cooling, was proposed in 1989 [?, 1] to explain experimentally measured cold atom cloud temperatures [?] which, at NIST in 1988, were found to be well below the expected limit obtainable by the well understood method of Doppler cooling³, one of the few examples of experiments turning out better than expected. A one dimensional theory has been developed [1] which has found remarkable agreement with three dimensional experiments [?]

One common configuration for Sisyphus cooling comprises two counterpropagating laser beams in each spatial dimension, both linearly polarised but with their polarisation angles perpendicular to one another. The optical field resulting from the two beams' superposition has regions of linear polarisation and of both helicities of circular polarisation, and varies between them on a length scale shorter than an optical wavelength.

The effect on multi-level atoms as they move from regions of one circular polarisation to another is that they are pumped alternately from one extreme of their spin-projection states to the other, alternately climbing and descending potential hills due to the dipole forces from the regions of different polarisations⁴. And so, like the Greek legend of Sisyphus⁵, who was doomed to push a rock uphill for eternity, the atoms are climbing hills repeatedly. Due to the state dependence of the strength of the dipole forces, the atoms climb steeper hills than they descend, and are thus slowed and cooled.

This type of cooling does not work in a magnetic field; the splitting of transition frequencies makes it impossible for an atom to traverse its spin manifold on one laser frequency. For this reason the Sisyphus cooling stage is performed with magnetic fields off, though a sufficiently short period is required such that the atoms can be recaptured when the trapping field is restored.

2.1.5 Evaporative cooling

The final stage of cooling is forced RF evaporative cooling [?, ?], which decreases the temperature of the cloud by systematically removing the hottest atoms. This is performed in a magnetic trap, which as mentioned earlier, only traps certain spin states. Evaporation proceeds by using an *RF knife* to induce spin flips in the atoms. The RF frequency is chosen such that it is only resonant with atoms some distance away from the center of the trap (via the Zeeman shift). The furthest out atoms are the most energetic, possessing the energy to climb the magnetic potential the furthest. By flipping their spins, these atoms are ejected due to the magnetic field becoming anti-trapping for them.

The cloud is given some time to rethermalise and the knife⁶ is moved inward where it removes slightly colder atoms. This is repeated until the desired compromise of lower temperature/lower atom number is reached. Usually some method is employed to prevent atoms near the center of the trap from undergoing spin flips [?] as they move across the field zero. The method we'll employ is to use an optical dipole trap in combination with the magnetic trap [?], such that the coldest atoms get trapped in the dipole trap which is offset from the magnetic field zero.

³As well as to explain other discrepancies between experiments and the theory of Doppler cooling, such as the optimal detuning of light being much greater than predicted.

⁴If you consider only one polarisation of light, its intensity varies sinusoidally in space, creating a series of potential hills and wells via the dipole force

⁵Polarisation gradient cooling is but one of a family of so called 'Sisyphus cooling' methods, all of which involve atoms repeatedly climbing potential hills.

⁶So called because it cuts the tail off the velocity distribution of the atom cloud.

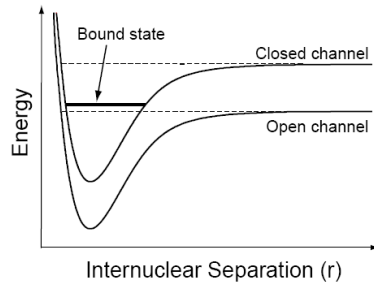


Figure 2.1: When atoms approach each other with spins aligned, they are in the *open channel*. In this channel they are unbound, but do not have enough energy to be free in the other channel - the *closed channel*. In the close range however, the atoms may have energy corresponding to a bound (molecular) state of the closed channel, a resonance which causes a divergence in the scattering length. The energy difference between the two channels can be tuned with a magnetic field and so these resonances can be induced in a wide range of situations.

2.1.6 Feshbach resonances

⁷Feshbach resonances can also be induced optically and with RF but magnetic resonances are the most commonly used.

A Feshbach resonance [?] is an enhancement of the interparticle interaction strength when a certain magnetic field strength is applied⁷. This phenomenon was first discovered in ultracold atoms in 1998 [?], and is now a staple of cold atom experiments.

The interparticle interaction mentioned above:

$$g = \frac{2\pi\hbar^2 a}{m_r} \quad (2.5)$$

where m_r is the reduced mass of a pair of the interacting particles, is dependent on a parameter a called the *s-wave scattering length*, which characterises low energy collisions between atoms. It is sensitive not only to what species of atoms are colliding, but also to their spin states. For each combination of spins, there is a different inter-atomic potential (called a *channel*) which determines the collision dynamics (Figure 2.1).

The resulting scattering length is sensitive to any bound states of this inter-atomic potential which are near the collision energy. If the channels of different spin states are coupled via the hyperfine interaction⁸, then the scattering length is also sensitive to bound states in the channels other than the one the atoms are in when they are far from each other. Due to the Zeeman effect, the energies between the different channels can be shifted with a magnetic field, and so a bound state can be shifted close to the collision energy, which causes the scattering length to diverge.

The end result is that at certain magnetic field strengths we find that atoms are much more strongly attracted to or repelled from each other.

We plan to use a Feshbach resonance (Figure 2.2) to enhance the interspecies repulsion between ⁸⁷Rb and ⁴¹K, thus trapping tracer particles more strongly in vortex cores.

2.2 Mean field theory: The Gross–Pitaevskii equation and vortices

Bose-condensates are described well by *mean field* theory, whereby the many-body wavefunction is approximated by a product of identical single-particle wavefunctions. Indeed, that the majority of the atoms are in the same quantum state is one of the defining features of BEC. The effect of interparticle interactions is included as a nonlinear term in the

⁸Requiring that the atoms in question have a nuclear magnetic moment.

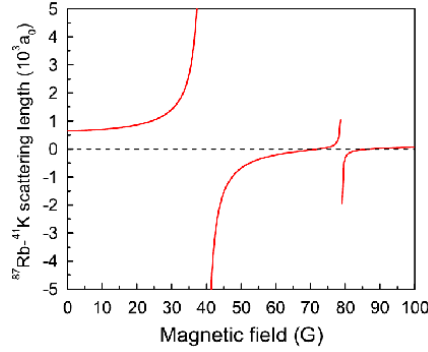


Figure 2.2: Predicted interspecies scattering length [?] as a function of magnetic field strength, for ^{41}K and ^{87}Rb both in their lowest energy hyperfine groundstate. The 35 gauss resonance is one of the main reasons for this pair of atoms being used in this project. It has a particularly low field strength and large width compared to most Feshbach resonances.

Schrödinger equation for the single particle wavefunctions, known as the Gross-Pitaevskii equation:

$$\frac{\partial \Psi}{\partial t} = \left[-\frac{\hbar^2}{2m} \nabla^2 + V(\mathbf{x}) + g|\Psi|^2 \right] \Psi, \quad (2.6)$$

where g characterises the strength of the interparticle interactions⁹, and $\Psi = \sqrt{N}\Psi_{\text{single}}$ is the single-particle wavefunction scaled by the square root of the number of particles¹⁰.

⁹And is usually positive—having the effect of stabilising BECs by self-repulsion.

In the hydrodynamic formulation of quantum mechanics [?], the flow velocity of a spatial wavefunction can be defined by considering the probability current to be a product of density and velocity. This allows us to define the superfluid velocity of a BEC as:

¹⁰Thus giving it the property that $|\Psi|^2$ is the particle density.

$$\mathbf{v} = \frac{\hbar}{m} \nabla \phi \quad (2.7)$$

where ϕ is the phase of the condensate wavefunction Ψ . Integrating this velocity over any closed path γ gives us the circulation:

$$C = \frac{\hbar}{m} \oint_{\gamma} \nabla \phi \cdot d\mathbf{s} \quad (2.8)$$

$$= \frac{\hbar}{m} 2\pi n, \quad n = 0, 1, 2, \dots \quad (2.9)$$

The fact that the circulation is quantised means that vorticity cannot exist in the condensate except in one-dimensional lines, about which the wavefunction's phase winds by a multiple of 2π . These topological defects are the quantised vortices that are central to this project.

At a vortex core, the atom density of a BEC must go to zero. This can be intuitively understood to arise from centrifugal forces, but is also required in order for the wavefunction to be continuous and single-valued across the core. This drop in density in the vicinity of a vortex core is what our method exploits in order to trap atoms within the cores.

2.3 Optical transitions on the ^{87}Rb D line

We atomic physicists do our theory work at an intermediate level of abstraction, at which many quantities and systems of interest can be computed and simulated with accurate models using standard quantum mechanics, but with the models not being fully a-priori. Instead, the Hamiltonians we feed to the machinery of standard quantum mechanics encapsulate some of the details we are not interested in or that are too hard to compute, with the link between the underlying layers of reductionism and the higher layer usually provided by experimentally measured constants rather than calculations from fundamental physics. In this way we can readily compute results about the atoms we are interested in by treating them as simpler systems than they actually are, with some of the the underlying details encapsulated by terms in an effective Hamiltonian for the dynamics that we are interested in.

In this section I'll summarise what the ^{87}Rb D line looks like from the perspective of a cold atom physicist, building up a Hamiltonian containing all 32 sublevels of the ground and first excited state of ^{87}Rb including fine structure, hyperfine structure, interaction with a magnetic field, and optical transitions between states. This Hamiltonian is the starting point for any calculations regarding cooling, trapping, and coherent control of ^{87}Rb , and the process for other alkali earth metals is much the same.

2.3.1 Fine structure

The rubidium 87 D line is not just one transition between a ground state and an excited state—there are two excited states, and the two resulting transitions are called, in order of their transition frequencies, the D_1 and D_2 lines. Thus the ground and first excited state of ^{87}Rb are actually a ground state plus two non-degenerate excited states, once we take into account fine structure. The groundstate is an S state (electronic orbital angular momentum quantum number $L = 0$), called the $S_{\frac{1}{2}}$ state, and the two excited states are P states ($L = 1$), one with the electron spin anti-aligned with its orbital angular momentum ($J = 1/2$) and one with the electron spin aligned with its orbital angular momentum ($J = 3/2$), called the $P_{\frac{1}{2}}$ and $P_{\frac{3}{2}}$ states respectively. In all of these states, ^{87}Rb 's single outer-shell electron occupies an orbital with principle quantum number $n = 5$, which for brevity we leave out of the notation. The transition between $S_{\frac{1}{2}}$ and $P_{\frac{1}{2}}$ is called the D_1 line, with experimentally measured (angular) transition frequency ω_{D_1} , and the transition between $S_{\frac{1}{2}}$ and $P_{\frac{3}{2}}$ is the D_2 line with angular transition frequency ω_{D_2} . These transition frequencies correspond to optical wavelengths of $\lambda_{D_1} \approx 795 \text{ nm}$ and $\lambda_{D_2} \approx 780 \text{ nm}$ [2].

This fine structure is treated entirely empirically for our purposes, and so our base Hamiltonian for the rubidium D line, taking into account only fine structure, is simply a statement of the experimentally measured energy differences between the states:

$$\hat{H}_{\text{fs}} = \hat{0}_{S_{1/2}} \oplus \hbar\omega_{D_1} \hat{1}_{P_{1/2}} \oplus \hbar\omega_{D_2} \hat{1}_{P_{3/2}}, \quad (2.10)$$

where $\hat{0}_{S_{1/2}}$, $\hat{1}_{P_{1/2}}$, and $\hat{1}_{P_{3/2}}$ are zero and identity operators each acting on the subspace of states within the $S_{\frac{1}{2}}$, $P_{\frac{1}{2}}$, or $P_{\frac{3}{2}}$ manifold, and \oplus is the direct sum.¹¹ The matrix representation H_{fs} of \hat{H}_{fs} in the basis in which it is diagonal (which we will call the $\{|L, J\rangle\}$ basis, since L and J are good quantum numbers for specifying one of the three states, which we otherwise write as L_J with the spectroscopic notation letter—S or P—corresponding

¹¹ Not to be confused with the Kronecker sum, with which it shares notation. The direct sum concatenates matrices as blocks, producing a larger, block-diagonal matrix with dimension equal to the sum of the dimensions of the matrices being direct-summed, whereas the Kronecker sum is the the regular sum of matrices after each has been multiplied using the Kronecker-product with identity matrices with sizes of the other matrices in the sum, producing matrices with dimension equal to the product of those being summed.

to the value of L in place of its numerical value) is

$$H_{\text{fs}} = \begin{bmatrix} \begin{bmatrix} \ddots & & \\ & 0 & \\ & & \ddots \end{bmatrix} & & \\ & \begin{bmatrix} \ddots & & \\ & \hbar\omega_{D1} & \\ & & \ddots \end{bmatrix} & \\ & & \begin{bmatrix} \ddots & & \\ & \hbar\omega_{D2} & \\ & & \ddots \end{bmatrix} \end{bmatrix}, \quad (2.11)$$

which is a block-diagonal matrix with each block also being a diagonal matrix. We have not yet specified the size of each submatrix—the size of each differs and depends on how many hyperfine and Zeeman sublevels are in that state.

This base Hamiltonian is worth pointing out since the energy differences between its three states are orders of magnitude larger than any of the energy differences between hyperfine and Zeeman sublevels within them. When doing any sort of calculations or simulations then, this time-independent Hamiltonian can be removed from the equations using an interaction picture, which we will come to shortly when we discuss optical transitions.

2.3.2 Hyperfine structure

Within each of the $S_{1/2}$, $P_{1/2}$ and $P_{3/2}$ states, the single outer-shell electron's total angular momentum $\hat{\mathbf{J}}$ has an interaction with ⁸⁷Rb's nuclear angular momentum $\hat{\mathbf{I}}$. This results in multiple discrete energy levels depending on the relative orientation of the two separate angular momenta. The interaction Hamiltonian for this hyperfine structure is [cite steck and the two references steck cites]¹²:

$$\hat{H}_{\text{hfs}} = \frac{A_{\text{hfs}}}{\hbar^2} \hat{\mathbf{I}} \cdot \hat{\mathbf{J}} + \frac{B_{\text{hfs}}}{\hbar^2} \frac{3(\hat{\mathbf{I}} \cdot \hat{\mathbf{J}})^2 + \frac{3}{2} \hat{\mathbf{I}} \cdot \hat{\mathbf{J}} - I(I+1)J(J+1)}{2I(2I-1)J(2J-1)}, \quad (2.12)$$

where J is the total angular momentum quantum number of the electron, equal to either $\frac{1}{2}$ or $\frac{3}{2}$ depending on which state in the D line we are considering, $I = \frac{3}{2}$ is the total angular momentum quantum number of the nucleus, and A_{hfs} and B_{hfs} are empirically determined coupling constants. Here we see the boundary between the quantities we can calculate with the machinery of quantum mechanics and those that we cannot and need to determine empirically—this expression applies so long as J and I are good quantum numbers,¹³ and the two terms are the dipolar and quadrupolar interactions [cite the review article] between two angular momenta, with the coupling constants determined empirically and encapsulating many details that are difficult to compute a-priori, such as relativistic effects and the exact shape of the electron orbitals given the presence of inner shell electrons. For the spherically-symmetric $S_{1/2}$ groundstate, there is no quadrupolar interaction and so B_{hfs} is only nonzero for the two P excited states.¹⁴ The values of A_{hfs} and B_{hfs} for each of the three states of the D line can be found in [steck].

For a given state of the D line, we can construct the matrix representation H_{hfs} of \hat{H}_{hfs} in the basis in which the z vector components \hat{I}_z and \hat{J}_z of $\hat{\mathbf{I}}$ and $\hat{\mathbf{J}}$ are diagonal by constructing matrix representations $\mathbf{I}_{I \times J}$ and $\mathbf{J}_{I \times J}$ of the operators $\hat{\mathbf{I}}$ and $\hat{\mathbf{J}}$ in that basis and then applying the expression (2.12). The subscript $I \times J$ on each of the matrices indicates that the matrix is a representation of its respective operator in the product space of the spaces I and J of the two individual nuclear and electronic angular momentum degrees of freedom.

To construct matrix representations of angular momentum operators in the product space $I \times J$, we first need their matrix representations \mathbf{I}_I and \mathbf{J}_J in their respective subspaces, which we will write as \mathbf{I} and \mathbf{J} for brevity. We can then expand the two operators into the total space by applying a Kronecker product with an appropriate identity matrix

¹²Note that this expression differs from those in the cited references by a factor of $1/\hbar^2$ —this is because I define the $\hat{\mathbf{I}}$ and $\hat{\mathbf{J}}$ angular momentum operators in SI units, rather than in units of \hbar^2 .

¹³ J is a good quantum number so long as the hyperfine splitting is small compared to the spacing between the three states of the D line, which it is, and I is a good quantum number so long as the hyperfine splitting is small compared to the energy difference between the groundstate and the first *nuclear* excited state, which it most certainly is.

¹⁴The quadrupolar term should be explicitly excluded from numerical computations of the hyperfine splitting on the $S_{1/2}$ state, as it contains a division by zero in this case, which may lead to erroneous results even if the term is subsequently multiplied by $B_{\text{hfs}} = 0$.

to each:

$$I_{T \times J} = I \otimes \mathbb{I}_J \quad (2.13)$$

$$J_{T \times J} = \mathbb{I}_T \otimes J \quad (2.14)$$

where \mathbb{I}_T is the matrix representation of the identity operator on the T subspace, equal to a $(2I + 1) \times (2I + 1)$ identity matrix, with \mathbb{I}_J defined similarly. Each of the two matrices is actually a vector of matrices, one for the angular momentum projection in each of the directions x , y and z . The procedure for constructing such matrices for arbitrary total angular momentum quantum numbers is as follows.¹⁵ I'll show the procedure for constructing J_x , J_y and J_z only for an arbitrary J , the procedure is identical for computing the vector components of I .

For a given total angular momentum quantum number J , the vector components of J in the z basis (the basis in which J_z is diagonal) can be constructed using the raising and lowering operators \hat{J}_+ and \hat{J}_- . Since the action of the raising and lowering operators on an eigenstate of J_z with angular momentum projection quantum number m_J is to produce an adjacent $(m_J \pm 1)$ eigenstate multiplied by a known constant [CITE SOME TEXTBOOK], this fact can be used to compute the nonzero matrix elements of \hat{J}_+ and \hat{J}_- in the $\{|m_J\rangle\}$ basis:

$$\langle m_J | \hat{J}_+ | m_J + 1 \rangle = \hbar \sqrt{J(J+1) - m_J(m_J + 1)}, \quad m_J < J, \quad (2.15)$$

$$\langle m_J | \hat{J}_- | m_J - 1 \rangle = \hbar \sqrt{J(J+1) - m_J(m_J - 1)}, \quad m_J > -J, \quad (2.16)$$

$$(2.17)$$

¹⁵We're using the standard convention of ordering the eigenvectors $\{|m_J\rangle\}$ in descending order of m_J . This is at odds with the computer programming convention of looping over most indices in ascending order, and so care should be taken when constructing these matrices in a computer program.

and therefore compute explicit matrices for J_+ and J_- in the $\{|m_J\rangle\}$ basis:¹⁶

$$J_+ = \begin{bmatrix} 0 & \dots & \dots & \dots & \dots & \dots \\ \langle J-1 | \hat{J}_+ | J \rangle & 0 & \dots & \dots & \dots & \dots \\ 0 & \langle J-2 | \hat{J}_+ | J-1 \rangle & 0 & \dots & \dots & \dots \\ \dots & 0 & \langle J-3 | \hat{J}_+ | J-2 \rangle & 0 & \dots & \dots \\ \dots & \dots & \dots & 0 & \dots & \dots \\ \dots & \dots & \dots & \dots & 0 & \langle -J | \hat{J}_+ | -J+1 \rangle \\ \dots & \dots & \dots & \dots & \dots & 0 \end{bmatrix}, \quad (2.18)$$

$$J_- = \begin{bmatrix} 0 & \langle J | \hat{J}_- | J-1 \rangle & 0 & \dots & \dots & \dots \\ \dots & 0 & \langle J-1 | \hat{J}_- | J-2 \rangle & 0 & \dots & \dots \\ \dots & \dots & \dots & 0 & \dots & \dots \\ \dots & \dots & \dots & 0 & \langle -J+2 | \hat{J}_- | -J+1 \rangle & 0 \\ \dots & \dots & \dots & \dots & 0 & \langle -J+1 | \hat{J}_- | -J \rangle \\ \dots & \dots & \dots & \dots & \dots & 0 \end{bmatrix}, \quad (2.19)$$

both of which have nonzero values along only one non-main diagonal adjacent to the main diagonal, and which form a Hermitian conjugate pair (or indeed, a transpose pair, since all elements are real). The matrix representations of \hat{J}_x and \hat{J}_y can then be computed by rearranging the defining expressions [CITE] for \hat{J}_+ and J_- :

$$\hat{J}_+ = \hat{J}_x + i\hat{J}_y, \quad (2.20)$$

$$\hat{J}_- = \hat{J}_x - i\hat{J}_y, \quad (2.21)$$

for \hat{J}_x and \hat{J}_y , and then applying the result to our matrix representations of \hat{J}_+ and \hat{J}_- to obtain matrix representations J_x and J_y of \hat{J}_x and \hat{J}_y in the $\{|m_J\rangle\}$ basis:

$$J_x = \frac{J_+ + J_-}{2}, \quad (2.22)$$

$$J_y = \frac{J_+ - J_-}{2i}. \quad (2.23)$$

Finally, since $\{|m_J\rangle\}$ is the eigenbasis of J_z with eigenvalues $\{\hbar m_J\}$, the matrix representation of J_z is simply the diagonal matrix of eigenvalues:

$$J_z = \begin{bmatrix} \hbar J & & & \\ & \hbar(J-1) & & \\ & & \ddots & \\ & & & \hbar(-J+1) \\ & & & & -\hbar J \end{bmatrix}. \quad (2.24)$$

We can also construct the matrix representation J^2 of the total (squared) angular momentum operator \hat{J}^2 as

$$J^2 = J_x^2 + J_y^2 + J_z^2, \quad (2.25)$$

or equivalently

$$J^2 = J(J+1)\hbar^2 \mathbb{I}_J, \quad (2.26)$$

since every m_J state is an eigenstate of the J^2 operator with eigenvalue $J(J+1)\hbar^2$.

The above prescription can be used to produce matrix representations of angular momentum operators J_x, J_y, J_z and J^2 for any integer or half-integer total angular momentum quantum number J . The three components can be considered a vector of matrices, J for the vector angular momentum operator \hat{J} . Below is a Python function that computes these matrices as well as the corresponding eigenvectors:

```

1 import numpy as np
2 hbar = 1.054571628e-34
3
4 def angular_momentum_operators(J):
5     """Construct matrix representations of the angular momentum operators Jx,
6     Jy, Jz and J2 in the eigenbasis of Jz for given total angular momentum
7     quantum number J. Return them, as well as the number of angular momentum
8     projection states, a list of angular momentum projection quantum numbers
9     mJ, and a list of their corresponding eigenvectors, in the same order as
10    the matrix elements (in descending order of mJ)."""
11    n_mJ = int(round(2*J + 1))
12    mJlist = np.linspace(J, -J, n_mJ)
13    Jp = np.diag([hbar * np.sqrt(J*(J+1) - mJ*(mJ + 1)) for mJ in mJlist if mJ < J], -1)
14    Jm = np.diag([hbar * np.sqrt(J*(J+1) - mJ*(mJ - 1)) for mJ in mJlist if mJ > -J], 1)
15    Jx = (Jp + Jm) / 2
16    Jy = (Jp - Jm) / 2j
17    Jz = np.diag([hbar*mJ for mJ in mJlist])
18    J2 = Jx**2 + Jy**2 + Jz**2
19    basisvecs_mJ = [vec for vec in np.identity(n_mJ)]
20    return Jx, Jy, Jz, J2, n_mJ, mJlist, basisvecs_mJ

```

Using the above prescription to construct a matrix representation of the \hat{J} operator with $J = \frac{1}{2}$ for the $S_{1/2}$ and $P_{1/2}$ states, or $J = \frac{3}{2}$ for the $P_{3/2}$ state, and to construct a matrix representation of the \hat{I} operator with $I = \frac{3}{2}$, we are close to being able to explicitly construct a matrix representation of the hyperfine interaction Hamiltonian for any state of the ⁸⁷Rb D line. The remaining step is to obtain the matrix representations of the two operators in the $\mathcal{I} \times \mathcal{J}$ product space using (2.13) and (2.14), and then we can apply (2.12) to our matrices to obtain the matrix representation H_{hfs} of \hat{H}_{hfs} for a given J corresponding to one of the three states on the D line:

$$H_{\text{hfs}} = \frac{A_{\text{hfs}}}{\hbar^2} \mathbf{I}_{\mathcal{I} \times \mathcal{J}} \cdot \mathbf{J}_{\mathcal{I} \times \mathcal{J}} + \frac{B_{\text{hfs}}}{\hbar^2} \frac{3(\mathbf{I}_{\mathcal{I} \times \mathcal{J}} \cdot \mathbf{J}_{\mathcal{I} \times \mathcal{J}})^2 + \frac{3}{2} \mathbf{I}_{\mathcal{I} \times \mathcal{J}} \cdot \mathbf{J}_{\mathcal{I} \times \mathcal{J}} - I(I+1)J(J+1)}{2I(2I-1)J(2J-1)}, \quad (2.27)$$

where the products of vector components within the dot products are computed with ordinary matrix multiplication. Alternatively, one can use the matrices in their individual

subspaces rather than their equivalents in the product space, so long as one interprets the dot products as “Kronecker dot products”:

$$H_{\text{hfs}} = \frac{A_{\text{hfs}}}{\hbar^2} \mathbf{I} \cdot \mathbf{J} + \frac{B_{\text{hfs}}}{\hbar^2} \frac{3(\mathbf{I} \cdot \mathbf{J})^2 + \frac{3}{2} \mathbf{I} \cdot \mathbf{J} - I(I+1)J(J+1)}{2I(2I-1)J(2J-1)}, \quad (2.28)$$

where \cdot is the Kronecker dot product:

$$\mathbf{I} \cdot \mathbf{J} \equiv I_x \otimes J_x + I_y \otimes J_y + I_z \otimes J_z. \quad (2.29)$$

In the above way one can construct an explicit matrix representation H_{hfs} for the hyperfine interaction for a given state of the D line. But what basis is it in? Because the matrix representations \mathbf{I} and \mathbf{J} of the electron and nuclear angular momentum operators were constructed in the $\{|m_I\rangle\}$ and $\{|m_J\rangle\}$ bases of their respective subspaces \mathcal{I} and \mathcal{J} , the matrices we have constructed in the product space $\mathcal{I} \times \mathcal{J}$ are in the basis $\{|m_I\rangle\} \times \{|m_J\rangle\}$ —the direct product of the two sets of basis vectors for the separate subspaces, with elements:

$$\{|m_I\rangle\} \times \{|m_J\rangle\} = \{|m_I, m_J\rangle \mid |m_I\rangle \in \{|m_I\rangle\}, |m_J\rangle \in \{|m_J\rangle\}\}, \quad (2.30)$$

where $|m_I, m_J\rangle = |m_I\rangle \otimes |m_J\rangle$ and \otimes is the direct product of vectors.¹⁷

The vector representation ψ of a state vector $|\psi\rangle$ in this basis is:

$$\psi = \begin{bmatrix} \langle m_I = I, m_J = J | \psi \rangle \\ \langle m_I = I, m_J = J - 1 | \psi \rangle \\ \vdots \\ \langle m_I = I, m_J = -J | \psi \rangle \\ \langle m_I = I - 1, m_J = J | \psi \rangle \\ \langle m_I = I - 1, m_J = J - 1 | \psi \rangle \\ \vdots \\ \langle m_I = -I, m_J = -J | \psi \rangle \end{bmatrix}. \quad (2.31)$$

The hyperfine Hamiltonian is not diagonal in the $\{|m_I, m_J\rangle\}$ basis. But, it is diagonal in the $\{|F, m_F\rangle\}$ basis, defined as the simultaneous eigenbasis of the \hat{F}^2 and \hat{F}_z operators, which are the total (squared) and z component of the total angular momentum operator $\hat{F} = \hat{\mathbf{I}} + \hat{\mathbf{J}}$, the matrix forms F^2 and F_z of which in the $|m_I, m_J\rangle$ basis can be constructed from the matrix forms of the individual angular momentum operators:

$$\begin{aligned} F_{\mathcal{I} \times \mathcal{J}} &= \mathbf{I}_{\mathcal{I} \times \mathcal{J}} + \mathbf{J}_{\mathcal{I} \times \mathcal{J}} \\ &= \mathbf{I} \otimes \mathbb{I}_{\mathcal{J}} + \mathbb{I}_{\mathcal{I}} \otimes \mathbf{J} \end{aligned} \quad (2.32)$$

$$\begin{aligned} F_{z \mathcal{I} \times \mathcal{J}} &= I_z \otimes \mathbb{I}_{\mathcal{J}} + \mathbb{I}_{\mathcal{I}} \otimes J_z \\ &= I_z \otimes \mathbb{I}_{\mathcal{J}} + \mathbb{I}_{\mathcal{I}} \otimes J_z \end{aligned} \quad (2.33)$$

$$F_{\mathcal{I} \times \mathcal{J}}^2 = F_{\mathcal{I} \times \mathcal{J}} \cdot F_{\mathcal{I} \times \mathcal{J}} \quad (2.34)$$

The $\{|F, m_F\rangle\}$ basis allows the eigenstates of the hyperfine interaction to be labelled with F and m_F quantum numbers. For a states of the ^{87}Rb D line with electron total angular momentum quantum number J , there are $1 + J + I - |(I - J)|$ hyperfine levels, with F quantum numbers running from $|I - J|$ to $J + I$. Within each hyperfine level there are $2F + 1$ degenerate states with different m_F quantum numbers ranging from $-F$ to F . This results in a total of 32 possible states for the rubidium D line, a schematic of which is shown in Figure 2.3.

¹⁷Although the symbol \otimes is used for both the Kronecker product and the direct product (of vectors), the direct product applies to vectors/state vectors, and the Kronecker product to matrices/operators. The direct product also applies to basis sets/spaces, but with the symbol \times . I would prefer nomenclature refer to them all with the same name and symbol, especially since the result of a direct product applied to an N -element column vector and an M -element column vector is identical to that of applying a Kronecker product to an $N \times 1$ matrix and a $M \times 1$ matrix, but I'll stick to the standard nomenclature.

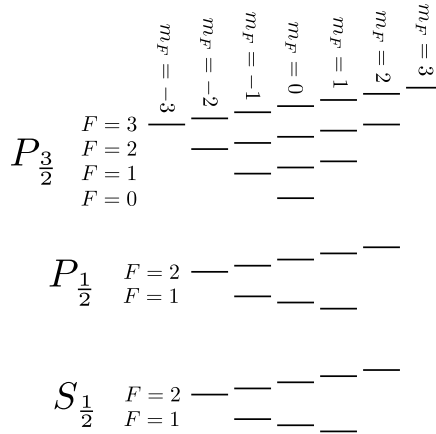


Figure 2.3: TODO: mention degeneracy of states and how F isn't a good quantum number

2.3.3 Zeeman sublevels

The states differing only in their m_F quantum numbers—called Zeeman sublevels—are degenerate in energy with respect to the hyperfine Hamiltonian, but an external magnetic field lifts this degeneracy. The Zeeman effect [CITE] results in an energy shift proportional to the external magnetic field \mathbf{B} and to a system's magnetic moment $\boldsymbol{\mu}$:

$$V = -\boldsymbol{\mu} \cdot \mathbf{B}. \quad (2.35)$$

Our atom is a composite particle, made of a nucleus with its own magnetic moment, an electron with its own spin, and a contribution from the orbital motion of the electron about the nucleus. Each magnetic moment is proportional to the angular momentum of the subsystem in question, with the proportionality constants, called Landé g -factors written as dimensionless multiples of $-\mu_B/\hbar$, where μ_B is the Bohr magneton.¹⁸ Since J is a good quantum number so long as energy shifts are smaller than the (large) energy spacing between the three main states of the D line, on the level we work we don't consider the electron spin and orbital angular momenta separately, rather we roll them into one with a single, empirically determined Landé g -factor g_J for the magnetic moment of the electron in each of the three states. Similarly we consider the nucleus as a single spin with an experimentally determined g_I , resulting in a Zeeman Hamiltonian:

$$\hat{H}_Z = -\hat{\boldsymbol{\mu}} \cdot \mathbf{B} \quad (2.36)$$

$$= -(\hat{\boldsymbol{\mu}}_I + \hat{\boldsymbol{\mu}}_J) \cdot \mathbf{B} \quad (2.37)$$

$$= \left(\frac{g_I \mu_B}{\hbar} \hat{\mathbf{I}} + \frac{g_J \mu_B}{\hbar} \hat{\mathbf{J}} \right) \cdot \mathbf{B}. \quad (2.38)$$

Separate g_S and g_L values are known and can be used in two terms instead of the one containing $\hat{\mathbf{J}}$ above if J is not a good quantum number, but in the regime we work that is not usually the case (and if it were, the fine and hyperfine structure Hamiltonians above would also be inadequate). If J is a good quantum number then it is more accurate to use the above expression with empirically measured g_J values, since they encapsulate QED effects and corrections due to the multi-electron structure of ⁸⁷Rb that are not captured by the simple Zeeman Hamiltonian with separate $\hat{\mathbf{S}}$ and $\hat{\mathbf{L}}$ terms.

If the energy shift from the Zeeman effect is small compared to the hyperfine splitting, then F is a good quantum number and a given hyperfine level can be treated as a single

¹⁸This is in the convention (that we use) where the Landé g -factor g_J for the electron is positive, otherwise the g -factors represent the proportionality constant as a multiple of $+\mu_B/\hbar$

magnetic moment subject to the Zeeman Hamiltonian:

$$\hat{H}_{Z\text{lin}} = \frac{g_F \mu_B}{\hbar} \hat{\mathbf{F}} \cdot \mathbf{B}, \quad (2.39)$$

where [cite steck]

$$g_F = g_J \frac{F(F+1) - I(I+1) + J(J+1)}{2F(F+1)} + g_I \frac{F(F+1) + I(I+1) - J(J+1)}{2F(F+1)}. \quad (2.40)$$

The direction in which each Zeeman sublevel shifts in energy for small magnetic fields is depicted in Figure 2.3. Experimentally, Zeeman shifts that depart from this linear regime are often encountered, and so it is an approximation that cannot always be made.

An explicit matrix representation H_Z of \hat{H}_Z in the $\{|m_I, m_J\rangle\}$ basis for each of the three states of the D line can be constructed by applying (2.38) to the matrix representations of $\hat{\mathbf{I}}$ and $\hat{\mathbf{J}}$ in that basis:

$$H_Z = -\boldsymbol{\mu} \cdot \mathbf{B}, \quad (2.41)$$

where

$$\boldsymbol{\mu} = -\frac{g_I \mu_B}{\hbar} \mathbf{I}_{I \times J} - \frac{g_J \mu_B}{\hbar} \mathbf{J}_{I \times J} \quad (2.42)$$

$$= -\frac{g_I \mu_B}{\hbar} \mathbf{I} \otimes \mathbb{I}_J - \frac{g_J \mu_B}{\hbar} \mathbb{I}_I \otimes \mathbf{J}. \quad (2.43)$$

2.3.4 Putting it all together

So far we have described how to construct a matrix representation of the fine structure Hamiltonian for the three main states of the ^{87}Rb D line, as well as matrix representations of each state's hyperfine and Zeeman Hamiltonians, these latter two in the same $\{|m_I, m_J\rangle\}$ basis. In the subspaces of each of the three main states then, we can sum together the matrix representations of the hyperfine and Zeeman Hamiltonians to form a matrix representation of the Hamiltonian taking both interactions into account:

$$H_{S_{1/2}} = H_{\text{hfs } S_{1/2}} + H_{Z S_{1/2}}, \quad (2.44)$$

$$H_{P_{1/2}} = H_{\text{hfs } P_{1/2}} + H_{Z P_{1/2}}, \quad (2.45)$$

$$H_{P_{3/2}} = H_{\text{hfs } P_{3/2}} + H_{Z P_{3/2}}, \quad (2.46)$$

where the subscripts $S_{1/2}$, $P_{1/2}$, and $P_{3/2}$ on the terms on the right hand side indicate that the expressions for the matrix representations of the hyperfine and Zeeman Hamiltonians are to be evaluated using the specific values of J , A_{hfs} , B_{hfs} , and g_I relevant to that state. The total Hamiltonian for the D line including fine structure, hyperfine structure and the Zeeman interaction is then

$$\hat{H} = \hat{H}_{\text{fs}} + (\hat{H}_{S_{1/2}} \oplus \hat{H}_{P_{1/2}} \oplus \hat{H}_{P_{3/2}}) \quad (2.47)$$

$$\Rightarrow \hat{H} = \hat{H}_{S_{1/2}} \oplus (\hbar\omega_{D_1} + \hat{H}_{P_{1/2}}) \oplus (\hbar\omega_{D_2} + \hat{H}_{P_{3/2}}), \quad (2.48)$$

the matrix representation of which in the $\{|L, J, m_I, m_J\rangle\}$ basis is the block diagonal matrix

$$H_{D^{87}\text{Rb}} = \begin{bmatrix} H_{S_{1/2}} & & \\ & [\hbar\omega_{D_1} + H_{P_{1/2}}] & \\ & & [\hbar\omega_{D_2} + H_{P_{3/2}}] \end{bmatrix}. \quad (2.49)$$

While $H_{D^{87}\text{Rb}}$ is a block diagonal matrix, each of the three submatrices is not diagonal, since m_I and m_J are not good quantum numbers for the hyperfine interaction (though

they are good quantum numbers for the Zeeman interaction and hence $H_{D^{87}\text{Rb}}$ becomes approximately diagonal at high magnetic field). Once one has constructed $H_{D^{87}\text{Rb}}$ or its submatrices, there are two other bases one might consider transforming the submatrices into depending on the circumstances. One is the $\{|F, m_F\rangle\}$ basis, in which the matrix representation of the hyperfine interaction is diagonal. The matrix representation of the Zeeman Hamiltonian is also approximately diagonal in the $\{|F, m_F\rangle\}$ basis, so long as one is in the linear Zeeman regime. Furthermore, the transition dipole moments for optical transitions are most easily calculated in the $\{|L, J, F, m_F\rangle\}$ basis, as we'll see in the next subsection. For these reasons the $\{|F, m_F\rangle\}$ basis is the most commonly used and referred to.

To transform each submatrix between the $\{|m_I, m_J\rangle\}$ and $\{|F, m_F\rangle\}$ bases, we use a unitary matrix whose elements are Clebsch–Gordan coefficients, each defined as the inner product of a $|F, m_F\rangle$ state with a $|m_I, m_J\rangle$ state (written in full as $|I, m_I, J, m_J\rangle$), and calculable as [CITE something]

$$\langle I, m_I, J, m_J | F, m_F \rangle = \begin{cases} (-1)^{I-J+m_F} \sqrt{2F+1} \begin{pmatrix} I & J & F \\ m_I & m_J & -m_F \end{pmatrix} & m_I + m_J = m_F \\ 0 & m_I + m_J \neq m_F \end{cases} \quad (2.50)$$

where the object in parentheses is a Wigner 3-j symbol. Given that the possible range of the F quantum number is from $|I - J|$ to $I + J$, and the possible range of m_F quantum numbers is from $-F$ to F for each F , an explicit construction of the unitary matrix U_{CG} of Clebsch–Gordan coefficients, in the convention where the column vectors in the $\{|F, m_F\rangle\}$ basis have F running from its highest value to lowest from top to bottom, and m_F also running from highest to lowest within each value of F , (omitting I and J for clarity) is:

$$U_{\text{CG}} = \begin{bmatrix} \langle m_I=I, m_J=J | F=I+J, m_F=F \rangle & \dots & \langle m_I=I, m_J=J | F=I+J, m_F=-F \rangle & \dots & \dots & \langle m_I=I, m_J=J | F=|I-J|, m_F=-F \rangle \\ \vdots & & \vdots & & & \vdots \\ \langle m_I=-I, m_J=-J | F=I+J, m_F=F \rangle & & \dots & & \dots & \langle m_I=-I, m_J=-J | F=|I-J|, m_F=-F \rangle \end{bmatrix}. \quad (2.51)$$

This the matrix that takes vectors from the $\{|F, m_F\rangle\}$ basis to the $\{|m_I, m_J\rangle\}$ basis, so its Hermitian conjugate U_{CG}^\dagger is needed for the inverse transformation. Each submatrix of the total Hamiltonian for the D line can be transformed into its $\{|F, m_F\rangle\}$ basis by using a unitary matrix of Clebsch–Gordan coefficients with the appropriate value of J , yielding a total Hamiltonian for the rubidium 87 D line in the $\{|L, J, F, m_F\rangle\}$ basis [TODO INDICATE BASIS ON MATRIX SOMEHOW]:

$$H_{D^{87}\text{Rb}}^{\text{ZF}} = \begin{bmatrix} U_{\text{CG}1/2}^\dagger H_{S1/2} U_{\text{CG}1/2} & & \\ & \hbar\omega_{D1} + U_{\text{CG}1/2}^\dagger H_{P1/2} U_{\text{CG}1/2} & \\ & & \hbar\omega_{D2} + U_{\text{CG}3/2}^\dagger H_{P3/2} U_{\text{CG}3/2} \end{bmatrix}, \quad (2.52)$$

where the additional subscripts on the unitary matrices indicates the value of J used in its construction. Armed with the $\{|F, m_F\rangle\}$ basis, we have little remaining reason to use the $\{|m_I\rangle, m_J\rangle\}$ basis any more. Even the Zeeman interaction, which can't

[TODO add i cross j as subscripts to all previous matrices in the mI, mJ basis, f subscripts to F matrices. When first mentioning the]

Here is a recap of what we have taken into account with our model of the Rubidium D line:

- The two lowest quantum numbers $L = 0$ and $L = 1$ of the electron's orbital angular momentum. This yields the S groundstate and P excited state.

- Fine structure: the two possible orientations of the electron's spin with respect to its orbital angular momentum. This splits the P excited state into two states, $P_{1/2}$ and $P_{3/2}$, and leaves the S groundstate as the single state $S_{1/2}$. The energies of these three states are determined entirely empirically—without any modelling of the fine structure.
- Hyperfine structure: The possible orientations of the electron's total angular momentum with respect to the nuclear angular momentum. This splits each state so far into $1 + J + I - |(I - J)|$ hyperfine states. The hyperfine interaction is treated semi-empirically, using an analytic form of the hyperfine interaction but with empirically determined coupling constants within each of the three states of the D line.
- Zeeman effect: the possible orientation of the total spin \hat{F} onto an external magnetic field. The Zeeman Hamiltonian is modelled analytically, but with empirically determined Landé g factors for each of the three states of the D line.

References

- [1] J. Dalibard and C. Cohen-Tannoudji. *Laser cooling below the Doppler limit by polarization gradients: simple theoretical models*. JOSA B **6**, 2023 (1989). DOI: [10.1364/JOSAB.6.002023](https://doi.org/10.1364/JOSAB.6.002023). [p 3]
- [2] D. A. Steck. Rubidium 87 D Line Data. steck.us/alkalidata, (2010). (revision 2.1.4). [p 6]

rev: 89 (d42828f15099)
author: Chris Billington
date: Tue Oct 17 17:39:06 2017 -0400
summary: Merge

This page intentionally left blank

Word count

Total

Words in text: 32979

Words in headers: 286

Words outside text (captions, etc.): 4690

Number of headers: 65

Number of floats/tables/figures: 31

Number of math inlines: 1171

Number of math displayed: 172

Files: 9

Subcounts:

text+headers+captions (#headers/#floats/#inlines/#displayed)
4635+52+783 (14/3/318/37) File(s) total: atomic_physics.tex
725+17+385 (4/4/7/0) File(s) total: experiment.tex
50+0+0 (0/0/0/0) File(s) total: front_matter.tex
1370+19+65 (3/2/39/13) File(s) total: hidden_variables.tex
1595+3+104 (2/0/12/0) File(s) total: introduction.tex
20562+152+2572 (30/15/716/118) File(s) total: numerics.tex
4+6+0 (1/0/0/0) File(s) total: software.tex
4002+24+781 (8/7/79/4) File(s) total: velocimetry.tex
36+13+0 (3/0/0/0) File(s) total: wave_mixing.tex

rev: 89 (d42828f15099)
author: Chris Billington
date: Tue Oct 17 17:39:06 2017 -0400
summary: Merge